Journal Pre-proof

In Situ Evolution of Electrocatalysts for Enhanced Electrochemical Nitrate Reduction under Realistic Conditions

Yingkai Chen, Jiayu Luo, Li Ling, Zhengshuo Zhan, Jiutan Liu, Zongjun Gao, Jason Chun-Ho Lam, Chunhua Feng, Yang Lei

PII: S2666-4984(24)00106-6

DOI: https://doi.org/10.1016/j.ese.2024.100492

Reference: ESE 100492

To appear in: *Environmental Science and Ecotechnology*

Received Date: 14 May 2024

Revised Date: 10 September 2024

Accepted Date: 11 September 2024

Please cite this article as: Y. Chen, J. Luo, L. Ling, Z. Zhan, J. Liu, Z. Gao, J.C.-H. Lam, C. Feng, Y. Lei, *In Situ* Evolution of Electrocatalysts for Enhanced Electrochemical Nitrate Reduction under Realistic Conditions, *Environmental Science and Ecotechnology*, https://doi.org/10.1016/j.ese.2024.100492.

Graphical Abstract for Article

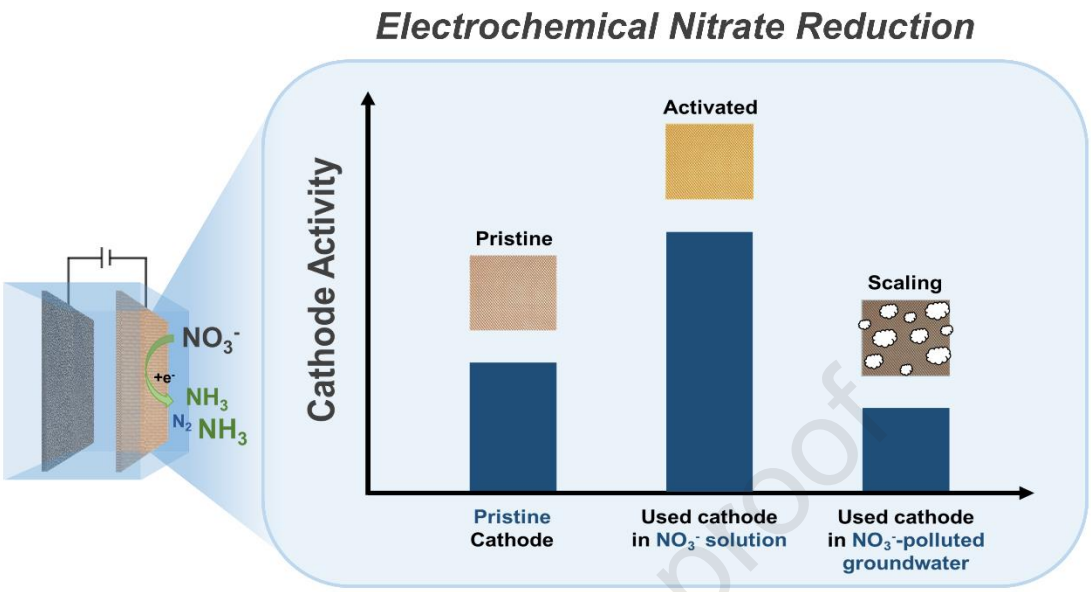

In Situ Evolution of Electrocatalysts for Enhanced Electrochemical Nitrate Reduction under Realistic Conditions

Yingkai Chen [a, b], Jiayu Luo [b], Li Ling [b], Zhengshuo Zhan [b], Jiutan Liu [c], Zongjun Gao [c], Jason Chun-Ho Lam [d], Chunhua Feng [a,*], Yang Lei [b,*]

[a] School of Environment and Energy, South China University of Technology, Guangzhou 510006, China

[b] Shenzhen Key Laboratory of Precision Measurement and Early Warning Technology for Urban Environmental Health Risks, School of Environmental Science and Engineering, Southern University of Science and Technology, Shenzhen 518055, China

[c] College of Earth Science and Engineering, Shandong University of Science and Technology, Qingdao, Shandong 266590, China

[d] School of Energy and Environment and State Key Laboratory of Marine Pollution, City University of Hong Kong, Hong Kong 999077, China

* Corresponding authors

E-mails: chfeng@scut.edu.cn (Prof. dr. Feng); leiy3@sustech.edu.cn (Prof. dr. Lei)

Abstract

Electrochemical nitrate reduction to ammonia (ENRA) is gaining attention for its potential in water remediation and sustainable ammonia production, offering a greener alternative to the energy-intensive Haber-Bosch process. Current research on ENRA is dedicated to enhancing ammonia selectively and productivity with sophisticated catalysts. However, the performance of ENRA and the change of catalytic activity in more complicated solutions (i.e., nitrate-polluted groundwater) are poorly understood. Here we first explored the influence of Ca^{2+} and bicarbonate on ENRA using commercial cathodes. We found that the catalytic activity of used Ni or Cu foam cathodes significantly outperforms their pristine ones due to the *in situ* evolution of new catalytic species on used cathodes during ENRA. In contrast, the nitrate conversion performance with nonactive Ti or Sn cathode is less affected by Ca^{2+} or bicarbonate because of their original poor activity. In addition, the coexistence of Ca^{2+} and bicarbonate inhibits nitrate conversion by forming scales ($CaCO_3$) on the *in situ*-formed active sites. Likewise, ENRA is prone to fast performance deterioration in treating actual groundwater over continuous flow operation due to the presence of hardness ions and possible organic substances that quickly block the active sites toward nitrate reduction. Our work suggests that more work is required to ensure the long-term stability of ENRA in treating natural nitrate-polluted water bodies and to leverage the environmental relevance of ENRA in more realistic conditions.

Keywords: Ammonium; *in situ* activation; hardness ions; groundwater; cathodic corrosion;

1. Introduction

Ammonia is intensively used to produce fertilizers, plastics, pharmaceuticals, and textiles, accounting for ~5% of the value of the worldwide chemical market (US$67 billion) [1]. Moreover, ammonia is attracting increasing interest as an energy carrier, given its high energy density (4.32 kWh L^{-1}) [2, 3]. Unfortunately, over 96% of NH_3 is produced via the energy-intensive Harbor–Bosch process, which consumes 5.5 EJ of global energy, representing about 11% of energy consumption in the chemical industry [2, 4]. The intensive use of NH_3 in agriculture and many other industries generates large amounts of nitrate-rich wastewater/groundwater [5, 6], requiring careful remediation or treatment (i.e., denitrification). Biological denitrification is currently the most frequently used process for dealing with nitrate-polluted wastewater. This process involves electron acceptors, which contribute to carbon emissions and waste nitrates in the form of N_2 [7]. Thus, nitrate reduction to ammonia represents an elegant strategy for achieving carbon-neutral and energy-saving ammonia production and water remediation [8].

In this context, electrochemical nitrate reduction to ammonia (ENRA) offers a promising route to mitigate the hazardous impacts of nitrate in bodies of water and to supplement the conventional energy-intensive Harber–Bosch method in producing ammonia [9, 10]. The electrochemical conversion of NO_3^- to NH_3 is a nine-proton coupled eight-electron transfer process, which suffers from sluggish reduction kinetics and forms many byproducts [11, 12]. While the exact mechanism of ENRA is still under intensive investigation, the scientific community generally accepts that it involves several steps, including nitrate adsorption to the electrocatalysts' surfaces, reduction to nitrite, and subsequent formation of ammonia through hydrogenation and deoxygenation [6, 12, 13]. Notably, many studies have identified that the rate-limiting step is the reduction of $*NO_3^-$ to $*NO_2^-$ (* refers to the active surface adsorbed) [14, 15].

Electrocatalysts are vital in determining faradaic efficiency, selectivity, and conversion efficiency in ENRA [13, 16]. Many researchers have devoted tremendous effort to improving the system's performance via rational catalyst selection and design. The most often practiced strategy for regulating ENRA's performance is to synthesize bimetal catalysts, such as Ru-Cu [17], Cu-Ni [18], and Cu-Co [14, 19], in which one metal favors nitrate reduction and the other favors atomic H* production, which is necessary to facilitate NH_3 formation through a tandem mechanism [14, 20]. Previous studies have shown that facet control and exposure [21], vacancy engineering [22], and single-atom catalysts [16,

23-25] are highly effective in modulating the selective formation of ammonia. For example, Zhang et al. achieved a maximum faradaic efficiency of 85%, a production rate of 1506 μg h^{-1} cm^{-2}, and a record-breaking ammonium selectivity of 99% with metal-organic framework-derived Co-doped Fe/Fe_2O_3 catalysts [26]. Notably, Chen et al. developed a Ru-dispersed Cu nanowire electrocatalyst, which delivers an industry-relevant nitrate reduction current of 1000 A m^{-2} while maintaining a high NH_3 faradaic efficiency of 93% for treating a 1000-mg L^{-1} nitrate solution [17]. The capability of ENRA for treating a dilute nitrate solution was demonstrated by Kim et al., who reported an outstanding NH_3 selectivity of 95.8% at 98.5% nitrate conversion and 96.8% faradaic efficiency at 0.2 V in 5 mM NO_3^- with a layered double hydroxide/Cu foam hybrid electrocatalyst [27]. Recently, Han et al. designed Ru_xCo_y alloys as model catalysts for ultralow overpotential nitrate reduction to ammonia. They proposed a three-step relay reduction mechanism, highlighting the importance of a spontaneous redox reaction between the Co metal and nitrate in producing the rate-limiting intermediate—nitrite [15].

The exciting performance of these pioneering catalysts in treating low nitrate-containing solutions demonstrates the environmental relevance of ENRA, as most nitrate-polluted water does not contain the high concentrations of nitrate that are tested in most studies, which typically range from concentrations of at least 50–1000 mM NO_3^- [5]. Nevertheless, the performance of these sophisticated catalysts has mainly been investigated in conventional two-chamber cells, and the durability of ENRA has been evaluated with pure nitrate-containing solutions over a relatively short period [8, 9, 12]. Few studies have fully considered environmental relevance when designing and evaluating novel catalysts for achieving ENRA, especially over long-term continuous flow operations in a single chamber cell instead of conventional H-type cells, which are challenging to translate to industrial applications [12, 28, 29].

Importantly, nitrate-polluted water bodies often contain many coexisting ions, among which calcium ions and (bi)carbonate are the most crucial cations and anions to consider. Unfortunately, only a few studies have evaluated the impact of Ca^{2+} and bicarbonate on ENRA's performance [30-32]. While two of the three previous studies concluded that the coexistence of Ca^{2+} and bicarbonate significantly worsened the performance of ENRA, these two studies reported different influences of bicarbonate. Huang et al. found that the performance of ENRA was negatively affected by bicarbonate but promoted by Ca^{2+} [31], while Atrashkevich et al. found that Ca^{2+} or bicarbonate alone

had a limited impact [30]. In contrast, Jian et al. concluded that both Ca^{2+} and (bi)carbonate had detrimental effects on the formation of ammonia [32]. In addition to these specific studies on the impact of coexisting ions, several studies have noted a significantly reduced performance of ENRA when treating actual wastewater (i.e., nitrate-polluted groundwater) [33, 34]. These few available studies inspired us to examine the influence of typical ions in depth.

Given that the purpose of this study was not to maximize the faradaic efficiency, product selectivity, or conversion efficiency of the ENRA system, we used commercial electrodes that have already demonstrated capability in pilot-scale applications [35] instead of the current state-of-the-art electrocatalysts, which vary from group to group. In addition, we did not focus on optimizing ENRA within the current setup and commercial electrodes. Our study aimed to reveal the influence of specific coexisting ions on the electrocatalytic performance of ENRA and to link the interactive mechanism at the surface–electrolyte interface, especially over long-term operations, with actual nitrate-polluted water bodies. We invite researchers to consider the importance of environmental relevance and work on solving the negative influence of coexisting ions over long-term continuous flow operations, mimicking industrial applications, which is urgently required before ENRA can be applied on a large scale.

2. Methods and Materials

2.1 Materials

We used commercial electrodes instead of the state-of-the-art single atom or nanocatalysts for possible upscaling. We acquired Ni and Cu foam (1 mm thickness) from Kunshan Longshengbao Electronic Material Co., Ltd. We obtained the Ti plate (1 mm thickness) from Qinghe Bodun Cemented Carbide Co., Ltd. and the Sn plate (1 mm thickness) from Dongguan Hongdi Metal Materials Co., Ltd. We utilized these four types of materials as cathodes. All the Ni and Cu foam cathodes were cut from a large piece of Ni or Cu foam. The pretreatment of the cathodes is detailed in Text S1 (Supplementary Material). While we used an IrO_2/RuO_2 plate (10×5×0.1 cm^3, Suzhou Shuertai Industrial Technology Co., Ltd., China) as the anode, we note that a cheaper graphite anode can be used when upscaling. We purchased sodium nitrate ($NaNO_3$, ≥99.0%) from Xilong Scientific Co., Ltd. (Guangdong, China), calcium nitrate ($Ca(NO_3)_2·H_2O$, ≥99.0%) from Sigma Aldrich, sodium bicarbonate ($NaHCO_3$, ≥99.8%) from

Shanghai Macklin Biochemical Co., Ltd. sodium sulfate (Na_2SO_4, ≥99.0%) from Shanghai Titan Scientific Co., Ltd., and ethanol (≥99.5%) from Sinopharm Chemical Reagent Co., Ltd. We prepared all test solutions with ultrapure water, unless specified.

2.2 Electrocatalytic nitrate reduction

We conducted the electrochemical nitrate reduction experiments in a single-chamber electrolytic cell fabricated with polymethyl methacrylate with a working volume of 0.5 L. The immersed areas of the cathode and anode were 4×4 cm^2 and 5×10 cm^2, respectively. The distance between the two electrodes was 1.5 cm. Based on preliminary experiments, the current density was set at 100 A m^{-2} for all tests, provided by a direct current power supply (0–16 V, MN-155D, Shenzhen Zhaoxin, China). Unless specified, the bulk solution always contained 4 mM $NaNO_3$ and 50 mM Na_2SO_4, with no pH adjustment. We applied a magnetic stirrer (SN-MS-1D, Shanghai Shangpu Instrument Equipment Co., Ltd.) at a stirring rate of 600 rpm to ensure uniform solute dispersion and facilitate mass diffusion.

An overview of the experimental conditions is provided in Table S1 (Supplementary Material). We first studied the influence of coexisting ions on the performance of electrochemical nitrate reduction with a Ni foam cathode. We then examined the role of cathode materials. Given that the cathode may be subject to *in situ* activation, we conducted a ten-cycle evaluation strategy for all tests. During the ten-cycle test, the cathode, anode, and reactor were thoroughly cleaned with deionized water after each cycle before running the following process. Notably, no acid or alkaline treatments were performed. We conducted all experiments at room temperature in an open atmosphere. We repeated each test ten times. However, we want to note that the cathodes underwent *in situ* activation; that is, the properties of the cathodes may have changed over time. Therefore, we present the results of all the ten-cycle tests instead of taking the conventional approach, which shows only the average plus standard deviation. We want to highlight the self-change in electrocatalytic nitrate activity, which has lacked attention in previous studies.

2.3 Analysis

We measured the bulk pH with a SevenExcellence™ pH meter (Mettler Toledo). We quantified the concentrations of NO_3^--N, NO_2^--N, and NH_4^+-N using an Agilent Cary 60 ultraviolet-visible (UV-vis) spectrophotometer and a HACH DR 3900 spectrophotometer

(Supplementary Materials Figs. S1–2). We analyzed the concentration of Ca, Mg and possible leaching metal ions using a Thermo Scientific inductively coupled plasma optical emission spectroscopy (ICP-OES) (iCAP7400 Duo MFC). In contrast, we measured anions using an ion chromatography system (Thermo Fisher Dionex AQuion) equipped with an AS-19 column.

2.4 Faraday Efficiency and Selectivity

We calculated the nitrate conversion efficiency according to equation (1). The selectivity of ammonia ($S_{NH_4^+}$) was calculated using equation (2).

$$\textit{Nitrate conversion}\ (\%) = \frac{C_{\mathrm{nitrate_0}} - C_{\mathrm{nitrate_t}}}{C_{\mathrm{nitrate_0}}} \times 100 \quad (1)$$

$$S_{\mathrm{NH_4^+}}\ (\%) = \frac{C_{\mathrm{ammonia_t}}}{\mathrm{C_{nitrate_0}} - C_{\mathrm{nitrate_t}}} \times 100 \quad (2)$$

In these equations, $C_{nitrate_0}$ is the nitrate concentration at the beginning of the experiment in mg NO_3^--N L^{-1}, $C_{\mathrm{nitrate_t}}$ is the nitrate concentration at time *t* in mg NO_3^--N L^{-1}, and $C_{\mathrm{ammonia_t}}$ is the ammonia concentration at time *t* in mg NH_4^+-N L^{-1}.

The faraday efficiency (FE) of electrocatalytic nitrate reduction was evaluated using equation (3):

$$\textit{FE}\ (\%) = \frac{\mathrm{n}\times\mathrm{F}\times N_{\mathrm{ammonia_t}}}{I\times 3600\times t} \times 100 = \frac{\mathrm{n}\times\mathrm{F}\times C_{ammonia_t}\times\mathrm{V}}{1000\times M_{\mathrm{ammonia}}\times I\times 3600\times t} \times 100 \quad (3)$$

In equation (3), *n* is the number of electrons required to generate ammonia per mole of ammonia (8 mol e^- per mol NH_4^+); F is the Faraday constant (96485 C mol^{-1}); $N_{\mathrm{ammonia_t}}$ and $C_{\mathrm{ammonia_t}}$ are the amount (mol NH_4^+) and the concentration (mg NH_4^+-N L^{-1}) of ammonia generated from electrochemical nitrate reduction, respectively; *I* is the applied current intensity (A); *t* is the electrolysis time (h); 3600 is a unit conversion factor (s h^{-1}); *V* is the volume of the electrolytic cell; M_{ammonia} is the molar mass of the ammonia; and 1000 is a unit conversion factor (mg g^{-1}).

2.5 Electrochemical analysis

We carried out the three-electrode electrochemical measurements using a CHI 750E electrochemical workstation (Shanghai Chenhua Instrument Co., China) with four types of electrodes (Ni foam, Cu foam, Ti plate, and Sn plate), Pt wire, and Ag/AgCl as the working electrode, counter electrode, and reference electrode, respectively. The potentials throughout this study were measured against Ag/AgCl (0.234 V vs. NHE) and converted

to the RHE scale ($E = E_{Ag/AgCl} + 0.234V + 0.0591pH$). Linear sweep voltammetry (LSV) and cyclic voltammetry (CV) were performed at a scan rate of 10 mV s^{-1} in a 0.05 M Na_2SO_4 solution with and without 4 mM $NaNO_3$. Electrochemical impedance spectroscopy (EIS) analysis was applied at 5 mV in a frequency range of 0.001–10000 Hz. We estimated the electrochemical surface area (ECSA) via the CV test by measuring the double-layer capacitance (C_{dl}).

2.6 Characterizations

We visualized the morphology and elemental composition of the fresh and used cathodes using a scanning electron microscope, followed by energy dispersive spectroscopy mappings at 15 kV (SEM-EDS, Thermo Fisher Scientific Quattro S). We identified the crystaline structure of deposits and/or the electrode via X-ray diffraction (XRD, Rigaku Smartlab) obtained within 2θ of 20–80° at an accelerating voltage of 40 kV and a current of 150 mA using a Cu Kα radiation source. In addition, *ex situ* grazing-incidence X-ray diffraction (GIXRD, Rigaku Smartlab) was used to identify the Ti plate electrode at grazing incidence angles of 0.5°. We also utilized X-ray photoelectron spectroscopy (XPS) (PHI 5000 Versaprobe III) to analyze the elemental compositions and valence states of all samples. All binding energies were calibrated using contaminant carbon (C 1s = 284.8 eV) as a reference. Raman spectra were collected in the 200–1200 cm^{-1} region with a resolution of 2 cm^{-1} and a laser beam with an excitation wavelength of 532 nm using a Laser Microscopic Raman Spectrometer (DXR3, Thermo Fisher).

3. Results and Discussion

3.1 Electrochemical nitrate reduction on nickel foam cathodes under different ion compositions

Our recent study showed that a Ni foam cathode performed well in a pilot-scale ENRA application [35]. Therefore, we initially selected Ni foam as a representative cathode material and studied the influence of Ca^{2+} and bicarbonate with synthetic solutions. We noted that the fresh and used Ni foam showed significantly different performances in catalyzing ENRA, indicating the *in situ* activation of Ni foam toward nitrate reduction [35]. In addition, no consistency was observed in our ten-cycle tests (Fig. 1a), suggesting that activation and/or deactivation occurs occasionally. Therefore, one must be cautious when making judgments/comparisons using a Ni foam cathode. Such inconsistencies may not

be restricted to Ni foam; many catalysts may share the same *in situ* activation/reconstruction as reported elsewhere [14, 20, 35, 36]. Therefore, we performed a ten-cycle test instead of duplicates or triplicates, as the standard deviation from the perspective of statistics does not truly reflect the performance of the Ni foam. In contrast, the changes we observed over the ten-cycle test reflected the differences in catalyst surface, morphology, crystal species, etc. Even so, it can be concluded that Ni foam can be self-activated during ENRA. Even after just one use, the electrocatalytic performance increased significantly. Although the performance fluctuated over the subsequent runs, it showed a deviation from 51.1% to 58.9% nitrate removal (Fig. 1a), with ammonia selectively of >77.5% under a constant current density of 100 A m^{-2} (Fig. 1d; Supplementary Materials Tables S2 and S3).

The *in situ* activation of the Ni foam cathode in ENRA was likely due to the formation of $Ni(OH)_2$ [35]. Both nitrate reduction and water electrolysis can lead to a localized region with a high pH around the Ni surface. A molten NaOH environment subsequently forms on the cathode surface in the presence of alkali metal ions, such as Na^+. Then, Ni on the cathode surface obtains electrons and is reduced to the negatively charged Ni^{x-} and immobilized by Na^+, called the Zintl phase. These ions are very reactive and can be highly susceptible to oxidation by H_2O to reform metal nanoparticles ($E_{Ni^{2+}/Ni}$= -0.257 V) and deposit them on the electrode surface, where they are subsequently oxidized by O_2 (E_{O_2/OH^-} = 0.806 V) to $Ni(OH)_2$ [35, 37]. In our case, XRD did not capture the presence of $Ni(OH)_2$ or any oxidized Ni species, presumably due to their amorphous nature (Fig. 1b). Nevertheless, SEM images suggested that the Ni foam surface changed after use (Fig. 1g–h). We noticed some tiny particles on the used Ni foam surface, which aligns with the results of other studies [38]. As a result, the surface becomes rough and may provide more active sites for nitrate reduction, supported by an enhanced electrochemical surface area (ECSA) from 0.119 to 0.169 mF cm^{-2} (Supplementary Materials Figs. S7–8). Moreover, EDS analysis confirmed that the newly formed nanoparticles contained more oxygen content (4.0 wt%) than the original Ni foam surface (0.3 wt%, Supplementary Material Fig. S4), suggesting the oxidation of Ni metal over ENRA. Therefore, we checked the surface functional groups of pristine and used Ni foam. Unfortunately, similar to XRD, Raman spectra did not identify the presence of $Ni(OH)_2$ (Fig. 1c). XRD and Raman typically probe beyond a depth of 100–1000 nm. This explains why they failed to recognize $Ni(OH)_2$, that is, due to the influence of background

Ni metal [39]. In contrast, XPS analysis can focus on a thickness of 1–10 nm; thus, it might be able to provide more information (Supplementary Material Figs. S5–6). Indeed, the XPS characterization revealed the presence of the lattice O in metal oxides at 529.4 eV, hydroxide O peak (Ni-O-H) at 530.9 eV, and chemisorbed O at 532.2 eV in the O 1s spectra and the Ni-OH peak in the Ni 2p spectrum (Fig. 1i–j), proving the formation of $Ni(OH)_2$ [35, 38, 40].

Unexpectedly, the presence of Ca^{2+} enhanced the performance of the fresh Ni foam. Nitrate removal in the first cycle with Ca^{2+} was 7.9% higher than without Ca^{2+} (Fig. 1a). The catalytic performance significantly improved after one use; in the second cycle, nitrate removal reached 25.9%. In subsequent cycles, nitrate removal gradually increased to 59.2%, with ammonia production selectivity of 89.6% (Fig. 2a; Supplementary Material Table S3). In the presence of Ca^{2+}, 2.5% nitrate-N was present as $CaNO_3^+$ (Supplementary Material Fig. S9), which likely promoted nitrate reduction on the Ni foam. The complex form $CaNO_3^+$ allows fast and easy nitrate migration toward the cathode surface [31]. Although only 2.5% is in the complexed form, the depletion of complexed nitrate shifts the formation of the new complex, thus continuously promoting the diffusion, migration, and reduction of nitrate on the cathode surface. In addition, the presence of Ca^{2+} condenses the thickness of the electric double layer near the cathode, facilitating the diffusion of the nitrate anion toward the cathode [41]. However, here the evolution of catalytic activity differed from that of the Ni foam in pure nitrate-containing conditions, in which the nitrate reduction activity quickly increased.

We also found that the Ca^{2+} concentration affected the system's performance (Supplementary Material Fig. S10). For the fresh Ni foam cathode, the nitrate removal performance increased from 7.0% without Ca^{2+} to 24.2% (0.5 mM Ca^{2+}) and 36.1% with 1.0 mM Ca^{2+}, then decreased to 14.8% with 2.0 mM Ca^{2+}. However, for the used Ni foam cathode (which was activated to some extent already), the presence of 0.5 (19.8%) or 2.0 mM Ca^{2+} (25.8%) inhibited nitrate removal. The nitrate removal performance slightly increased with 1.0 mM Ca^{2+} (59.2%) than without Ca^{2+} (55.7%). These results indicate that the presence of Ca^{2+} might also affect the *in situ* activation of the Ni foam cathode, thereby exhibiting a mixed influence on the fresh and used cathodes. A possible explanation is that Ca^{2+} competes with Ni^{2+} toward OH^-, thus slowing the evolution of active $Ni(OH)_2$ and nitrate reduction.

As in the case in which Ca^{2+} is absent, XRD and Raman did not provide helpful

information in exploring the change in the Ni foam surface (Fig. 1b–c). However, SEM-EDS and XPS provided solid evidence pointing to the formation of new nanoparticles on the cathode surface, including enhanced oxygen content (3.2 wt%) (Fig. 2d; Supplementary Material Fig. S4) and the evolution of $Ni(OH)_2$ (Fig. 2g). Moreover, the electrochemical impedance spectroscopy (EIS) curve of the used Ni foam in the presence of Ca^{2+} showed lower charge transfer resistance (R_{ct}) than the fresh Ni foam (Fig. 1f), indicating enhanced kinetics of electrode reactions after use [42]. Also, the ECSA of the used Ni foam (0.292 mF cm^{-2}) was 2.5 times higher than that of the fresh Ni foam (0.119 mF cm^{-2}) (Supplementary Materials Figs. S7–8). Likewise, the LSV curve demonstrated an enhanced current signal using Ni foam (Fig. 1e).

In contrast to the influence of Ca^{2+}, bicarbonate significantly inhibited the removal of nitrate and the formation of ammonia during the first cycle (Fig. 1a, Fig. 2b). Nonetheless, after use, the catalytic activity of the Ni foam improved substantially, achieving 2.0% nitrate removal for the fresh Ni foam compared to 54.5% removal in the second cycle. These results suggest that Ni foam's *in situ* activation vastly outperforms bicarbonate's inhibiting impact. To date, only a few studies have examined the influence of bicarbonate. Our finding is consistent with [31, 32], and [34] but contrasts with the results of [30]. The negative impact of bicarbonate is likely due to its competition with nitrate toward the active site [33]. Bicarbonate is a complex anion that can form precipitates with active catalyst sites after deprotonation. Given that the cathode has a locally high pH, bicarbonate tends to consume OH^- and become deprotonated (carbonate), which may easily occupy the activate site via metal carbonate precipitation (i.e., K_{sp} of $NiCO_3$ is 1.42×10^{-7}).

Indeed, we found that the used Ni foam turned light green (Supplementary Material Fig. S3) and developed some newly formed nanoparticles on the surface (Fig. 2d–e). The corresponding Raman (Fig. 1c) and XPS spectra (Fig. 2g; Supplementary Material Fig. S6) confirmed the presence of $Ni(OH)_2$ and $NiCO_3$. Specifically, the Raman spectrum peaked at approximately 454 and 970 cm^{-1} were assigned to $Ni(OH)_2$ [43]. In contrast, the signal peak at around 1080 cm^{-1} was associated with symmetric stretching of the CO_3^{2-} group [44]. Moreover, the CO_3^{2-} group was observed in both C 1s and O 1s in the XPS spectrum (Fig. 2g; Supplementary Material Fig. S6). Consistently, the surface became rough, with an enlarged ECSA from 0.119 to 0.139 mF cm^{-2} (Supplementary Material Fig. S7).

The coexistence of bicarbonate and Ca^{2+} reduced nitrate reduction from 50–60% to 15–38% and inhibited the production of ammonia (Fig. 1d, Fig. 2c). This was probably due to another mechanism: cathode scaling and the complete blocking of active sites for electrochemical nitrate reduction [30, 31, 33]. SEM images of the used Ni foam showed that the surface was covered with cubic crystals (calcite) (Fig. 2f). The formation of $CaCO_3$ is further supported by the relevant XRD and Raman spectra (Fig. 1b–c). In addition, the decrease in Ca^{2+} concentration after treatment reflected the precipitation of Ca^{2+} exactly (Supplementary Material Table S4). Cathode scaling is a significant issue in electrochemical nitrate reduction, as nitrate is typically present at much lower concentrations than Ca^{2+} and bicarbonate. In ENRA, both the desired nitrate reduction reaction and the competing H_2 evolution reaction will produce hydroxide, which results in a significantly locally higher pH near the cathode than the bulk solution [45]; the bulk pH is also enhanced from 7.0–7.5 to about 11.0–11.5 (Supplementary Material Table S2). It should be noted that no bulk precipitation was observed, although the bulk solution was highly saturated with $CaCO_3$, which indicates that the cathode surface had a favorable environment for $CaCO_3$ deposition. Therefore, beyond developing novel catalysts, we should also consider the elimination of the negative impacts of scaling ions. For example, a pretreatment could be applied to remove these hardness ions [30, 33] or a novel system could be designed to achieve simultaneous nitrate reduction and hardness control [46].

3.2 Influence of cathode material

Whether the influence of the cathode material is limited to Ni foam was of interest. Therefore, we studied four materials representing two types of cathode, one termed activate cathode (Ni and Cu foam) [35, 47], which likely undergoes *in situ* activation, as reported. The other is the inactive cathode (Ti or Sn plate) [30, 48]. The peaks in the LSV curves at −0.35 to −0.55 V corresponded to the response current intensity of the different electrodes to nitrate reduction (Fig. 3b). The response current in the absence of nitrate corresponded to the hydrogen evolution reaction (HER) for all four electrodes. After adding nitrate, we noticed a significant increase in the current intensity, indicating nitrate reduction. Therefore, we concluded that the current output was mainly attributed to nitrate reduction.

Interestingly, for the active cathode group, the pristine cathodes showed much less catalytic activity than the used cathodes (Fig. 3a; Supplementary Material Fig. S11). Notably, the fresh Cu foam exhibited slightly better activity than the new Ni foam,

suggesting its inherent activity toward nitrate reduction. Still, the catalytic activity of the Cu foam increased even after just one use, which was accompanied by enhanced surface roughness and oxygen content (Supplementary Material Fig. S13), increased ECSA (Fig. 3c), and lowered R_{ct} (Fig. 4g). The LSV curve of the used Cu foam also exhibited a much higher current output than the fresh one under the same conditions (Fig. 3b). These results collectivity confirmed the enhanced activity of the used Cu foam during ENRA [49].

In contrast, these phenomena were not observed in the Ti and Sn cathodes. We did not observe significant improvement with the used nonactive cathodes compared with the new cathodes. To be precise, the Sn plate showed the worst performance under all the studied conditions (Fig. 3a), possibly due to a large overpotential under the tested conditions (Fig. 4f). Unlike the noted enhanced catalytic activity after use, the Sn electrode experienced a quick decrease in the system's performance. For example, in the case of a nitrate-only solution, the system removed about 34.2% of the nitrate after 6 h of electrolysis at 100 A m^{-2}. However, this value dropped to 20.0% in the second cycle and 10.5% in the 10th cycle. In contrast, the Ni and Cu foam cathodes typically achieved 60–80% nitrate removal efficiency.

Therefore, it seems reasonable to speculate that the type of cathode material also matters. Due to the large overpotential toward competitive HER, Ni and Cu foam are widely used for electrochemical nitrate reduction reactions. In addition, some studies have used Ni or Cu foam as a base material in which different types of catalysts (i.e., single-atom catalysts) are decorated on the surface of Ni or Cu foam [39, 50, 51]. However, no previous study has considered the *in situ* activation mechanism. Instead, they typically argue that Ni- or Cu-supporting matrixes have limited catalytic activity toward nitrate reduction to ammonia [20, 39, 52]. In contrast, in the current study, we showed that these supporting electrodes may be subject to *in situ* activation, thus demonstrating outstanding activity in ENRA, and should not be ignored. Therefore, the *in situ* activation phenomenon should be considered when discussing the mechanisms or impacts of other parameters.

Nonetheless, we want to point out that the Ti cathode—the nonactive electrode—is also subject to *in situ* modification [48, 53]. The used Ti electrode surface became rough (Supplementary Material Fig. S22), with increased ECSA from 0.0247 to 0.0691 mF cm^{-2} (Fig. 3d) and reduced R_{ct} (Fig. 4h). In addition, the LSV curve of the used Ti plate showed a higher current response than the new one under the same conditions (Fig. 3b). Moreover, the associated XRD spectrum confirmed the formation of TiH_2 (Fig. 3g). Likewise, the Sn

electrode also underwent some *in situ* modifications, such as the occurrence of SnO_2 nanoparticles on the cathode surface (Fig. 3h; Supplementary Material Fig. S27) with enhanced ECSA from 0.0138 to 0.0549 mF cm^{-2} (Fig. 3e) and reduced R_{ct} (Fig. 4i). These results clearly showed the evolution of the Ti and Sn surfaces in terms of speciation, morphology, and elemental composition over the ENRA process, which might correlate with the changes in electrochemical nitrate reduction performance during the ten-cycle test. Notably, the *in situ* modification of nonactive electrodes did not significantly affect their electroactivity (Supplementary Materials Fig. S21, Fig. S26, and Tables S7–10), as found elsewhere [53, 54].

3.3 Joined effects of coexisting ions and cathode material

Regarding the influence of coexisting ions, bicarbonate weakened the nitrate reduction activity of the fresh Cu, Ni, and Ti cathodes but not that of the Sn cathode (Fig. 1a, Fig. 4a–c), which was confirmed by the relevant LSV curves (Fig. 4d–f). It is worth mentioning that the peaks at −0.35 to −0.55 V vs. RHE for the Cu foam, Ti plate, and Sn plate in the LSV curve corresponded to direct electron transfer for nitrate reduction [52, 55-57]. In comparison, a noticeable reduction peak was observed at −0.85 V vs. RHE in the LSV curve of the Sn plate, which was attributed to the transition between Sn(0) and Sn(II) [56]. In addition, appropriate material characterization suggests that some modifications occurred on the cathode surface in the presence of HCO_3^- (Supplementary Materials Fig. S17, Fig. S23, and Fig. S29). This is probably why two previous studies have drawn different conclusions about the role of bicarbonate, as a Cu cathode was used in one study [31], while an Sn cathode was used in another study [30].

As discussed previously, Ca^{2+} can potentially influence electrochemical nitrate reduction by affecting the thickness of the electric double layer and forming complexes with nitrate. Unlike Ni foam, the presence of Ca^{2+} weakens the activity of Cu foam toward nitrate reduction (Fig. 4b; Supplementary Material Tables S5–6), which is reflected by the decreased ECSA from 0.139 to 0.0669 mF cm^{-2} (Supplementary Materials Figs. S19–20). It seems that the *in situ* construction of Cu foam is somehow affected or driven in a way that does not favor nitrate reduction. The photo of the Cu foam shows visible color changes, indicating some modification of the Cu foam (Supplementary Material Fig. S12). The SEM-EDS spectrum shows the rougher surface and high oxygen content of the Cu foam (Supplementary Material Fig. S13). In addition, based on the XPS and XRD survey

(Supplementary Materials Figs. S14–16), the used Cu foam exhibited signals of Cu_2O as does in pure nitrate-containing solution (Fig. 3f), the leading active site for H_2O dissociation and *H production [58]. The produced *H could facilitate nitrate reduction via indirect electron transfer [52, 59]. Further research is required to confirm the presence of *H within non-noble metal catalysis. In addition, Ca^{2+} negatively affected the performance of the Ti plate in the ENRA process, as evidenced by a decrease in nitrate removal from 56.3–71.2% to 26.5–61.4% and reduced ECSA from 0.0691 to 0.0301 mF cm^{-2} (Supplementary Materials Figs. S24–25). The XRD characterization identified the generation of TiH_2 on the Ti plate surface (Supplementary Material Fig. S23). Significantly, the evolution of TiH_2 may also be linked to *H. However, no study has yet clarified the pathway of TiH_2 generation and its catalytic activity toward nitrate reduction.

We believe that the unique influence of Ca^{2+} is tied to the nitrate reduction mechanism with different cathodes. Where the direct electron transfer mechanism dominates, it promotes nitrate reduction, whereas it inhibits nitrate reduction in systems in which indirect *H reduction matters. Janik and colleagues simulated the hydrogenation of *CO to form *COH in the Cu(111) facet using DFT. They argued that the presence of K^+ increases the energy barrier for producing *COH because the electrostatic repulsion between the *H and K^+ hinders the movement of H^+ and its binding with *CO [60]. Likewise, in the current study, the presence of Ca^{2+} may have affected the adsorption of *H on the cathode. This combination of non-reactive cations (i.e., Ca^{2+}) and *H is vital as it could help clarify their distinct impact on electrocatalytic nitrate reduction with different cathodes.

Surprisingly, in the case of the Sn cathode, electrochemical nitrate reduction was strongly favored in the presence of Ca^{2+} compared to the other cathodes (Fig. 4c), confirmed by the relevant LSV curves (Fig. 4f) and the ECSA analysis (Supplementary Materials Figs. S31–32, Tables S11–12). Moreover, we found SnO_2 particles on the Sn surface (Fig. 3h; Supplementary Material Fig. S28). Specifically, electrochemical nitrate removal was enhanced by at least 20%, jumping between 38% and 52% over the ten-cycle test. This may have been due to the direct electron transfer mechanism and the active effect of the higher charge density of Ca^{2+}, which led to a remarkable shift in the potential and promoted nitrate reduction. Additionally, the hydrated calcium ion $[Ca(H_2O)_6]^{2+}$ is a proton donor by several orders of magnitude stronger than water molecules in the bulk solution, which may also have contributed to the promotion of nitrate reduction [61].

In the presence of both Ca^{2+} and bicarbonate, regardless of the cathode material, nitrate reduction performance was negatively affected. The primary reason was the blocking of active sites created by $CaCO_3$ deposition (Supplementary Materials Fig. S18, Fig. S23, and Fig. S30), which hindered the metal binding with nitrate, thus inhibiting nitrate reduction to ammonia [30, 31]. Interestingly, when comparing the effects of $CaCO_3$ deposition in the two types of cathodes, the negative influence of $CaCO_3$ deposition was more significant with the plate electrodes. For instance, the ENRA performance with a Ti cathode was significantly reduced from 80% to less than 20% with the coexistence of Ca^{2+} and bicarbonate (Fig. 4b), likely due to the limited surface area and its being blocked by $CaCO_3$ deposition. In contrast, porous Ni and Cu foams have large surface areas and more active sites for nitrate reduction and $CaCO_3$ deposition. Therefore, after one cycle, $CaCO_3$ deposition did not influence nitrate reduction. Nonetheless, there was significant $CaCO_3$ accumulation on the cathodes over the ten rounds of recycling. Therefore, the negative influence of $CaCO_3$ deposition became apparent later (after three rounds of recycling).

For the Sn plate, with the coexistence of Ca^{2+} and bicarbonate, the system's performance was also poor but relatively stable over the ten-cycle test, ranging from 22% to 34%. It is unclear what caused the different behavior of the Sn electrode compared to other electrodes in the ENRA process. The contrasting results indicate the need for further research to identify the distinct behavior of Sn electrodes. However, as we confirmed in the current study, regardless of the material, all cathodes were subject to *in situ* modifications, which was likely the actual reason for the *in situ* activation of some catalysts over reduction applications.

Overall, we can conclude that all cathodes underwent an evolution of new species, but not all were able to enhance the catalytic activity of ENRA. The influence of coexisting ions on the performance of ENRA was also affected by the nature of the electrocatalysts (the cathode material). Moreover, we need to consider the *in situ* modification phenomenon when interpreting the mechanisms of new or existing electrocatalysts in the ENRA process. We suggest applying *in situ* characterization techniques to probe the evolution of active species, which could more accurately link the activity change with the formation of new species on raw materials.

3.4 Long-term performance of the best-performed Cu foam

We conducted a long-term evaluation with the best-performing Cu foam over two months to gain insights into the system's performance over continuous flow operations and to mimic its practical application. To our knowledge, few previous studies have attempted to evaluate the long-term stability of ENRA in nitrate-polluted water bodies [8, 9]. Fig. 5a presents the nitrate removal efficiency over a continuous flow operation for treating three types of nitrate-containing solutions, including pure nitrate-containing solutions synthesized with deionized water, more environmentally relevant nitrate-containing solutions prepared with tap water (Supplementary Material Table S13), and actual nitrate-polluted groundwater (Supplementary Material Table S14). Figure 5a shows that the system quickly reached an enhanced nitrate removal of about 12.7% for the natural groundwater. However, after several days of operation, we noticed a substantial decrease in pH, nitrate removal, and ammonia production (Supplementary Materials Tables S15–16).

The worst performance in treating nitrate-contaminated groundwater was likely due to the abundance of hardness ions (14.7 mM Ca^{2+} and 5.9 mM Mg^{2+}). Fig. 5d reveals the apparent removal of Ca and Mg via electrochemical groundwater treatment. The corresponding XRD analysis showed noticeable scaling on the Cu foam surface (Fig. 5c), which may have prevented direct contact between nitrate and the active Cu sites. In addition, coexisting dissolved organic matter, silicate, and other ions may have affected nitrate reduction performance [33, 46]. The tap water tests, which contained fewer hardness ions and other components, showed an enhanced operation period (15 d vs. 3 d in groundwater) with a stable hardness removal (Supplementary Material Fig. S33) before decreasing in nitrate reduction.

In contrast, the system's performance in pure nitrate-containing solutions lasted much longer before an apparent decrease in nitrate removal. This distinction indicates that future studies should evaluate the stability of electrochemical nitrate reduction systems under environmentally relevant conditions. Otherwise, the evaluation cannot predict the actual stability or performance of the electrochemical nitrate reduction system. Significantly, the appearance of the Cu foam used under long-term continuous flow operations changed from golden yellow to black (Supplementary Material Fig. S34), powerfully demonstrating the *in situ* modification of the Cu foam cathode. The relevant XRD characterization revealed the formation of Cu_2O (Fig. 5b). To our knowledge, this is the first study demonstrating the *in situ* modification of cathode material in the context of

ENRA on a macro scale, adding value to previous studies that have mainly focused on nano-scale changes. In addition to nitrate removal efficiency, we quantified the relevant energy consumption (Supplementary Material Table S17). The specific energy consumption was 138.38, 465.50, and 1118.28 kWh per kg N for pure nitrate solution, nitrate spiked tap water, and natural groundwater, respectively, implying that coexisting ions and organic substances affected energy consumption beyond stability.

Further studies on the influence of many other ions, such as Mg^{2+}, SiO_3^{2-}, and natural organic matter, typical ions and substances found in groundwater, agriculture runoff, and industrial wastewater, are urgently required. In the meantime, we hope that the current study can provide a foundation and encouragement for scientists to consider the environmental relevance of electrochemical nitrate reduction, as this is urgently needed to replace the high-temperature, high-pressure Harbor–Bosch process in producing ammonia. If environmental significance cannot be guaranteed, these sophiscated catalysts are unlikely to be applied to industrial-grade wastewater. Alternatively, consideration could be given to the reduction of nitrogen, which can easily be acquired from the air, although scientists are well aware of the challenge involved in breaking the stable N≡N bond (941 kJ mol^{-1}) rather than the N-O bond (204 kJ mol^{-1}) [62]. Therefore, we recommend that future studies evaluate the environmental relevance of state-of-the-art electrocatalysts.

4. Conclusion

To summarize, we have outlined the critical importance of considering environmental relevance when evaluating the performance of new or existing electrocatalysis for nitrate reduction to ammonia, especially during long-term operations under wastewater-relevant conditions. While pure nitrate solutions can be useful for evaluating mechanisms, our findings demonstrate that typical coexisting ions significantly influence electrocatalytic performance. Beyond scaling formations that block active sites, coexisting ions also affect the *in situ* activation of the cathode. Therefore, we strongly suggest that researchers consider coexisting ions or substances, as they profoundly affect the activity and long-term stability of electrocatalysts toward nitrate reduction to ammonia. We strongly encourage further research aimed at mitigating the negative influence of coexisting substances.

CRediT author statement

Yingkai Chen: Methodology, Formal Analysis, Investigation, Data Curation, Writing - Original Draft, Visualization. **Jiayu Luo:** Software, Investigation, Resources, Data Curation. **Li Ling:** Validation, Resources, Visualization. **Zhengshuo Zhan:** Methodology, Validation. **Jiutan Liu:** Resources. **Zongjun Gao:** Resources. **Jason Chun-Ho Lam:** Writing - Review & Editing. **Chunhua Feng:** Conceptualization, Writing - Review & Editing, Supervision. **Yang Lei:** Conceptualization, Methodology, Writing - Review & Editing, Project Administration, Funding Acquisition.

Declaration of competing interest

The authors declare that they have no known competing financial interests or personal relationships that could have appeared to influence the work reported in this paper.

Acknowledgments

This work was financially supported by the Shenzhen Science and Technology Program (JCYJ20230807093405011; 20220815101937003), Guangdong Basic and Applied Basic Research Foundation (2023A1515110152), and the Shenzhen Key Laboratory of Precision Measurement and Early Warning Technology for Urban Environmental Health Risk (ZDSY20220606100604008), the High Level of Special Funds (G03050K001). The authors thank SUSTech Core Research Facilities for their assistance.

Supplementary Material

The supplementary material is available free of charge at the publisher's website.

References

[1] K. Fan, W. Xie, J. Li, Y. Sun, P. Xu, Y. Tang, Z. Li, M. Shao, Active hydrogen boosts electrochemical nitrate reduction to ammonia, Nature Communications, 13 (2022).

[2] C. Smith, A.K. Hill, L. Torrente-Murciano, Current and future role of Haber–Bosch ammonia in a carbon-free energy landscape, Energy & Environmental Science, 13 (2020) 331-344.

[3] G.-F. Chen, Y. Yuan, H. Jiang, S.-Y. Ren, L.-X. Ding, L. Ma, T. Wu, J. Lu, H. Wang, Electrochemical reduction of nitrate to ammonia via direct eight-electron transfer using a copper–molecular solid catalyst, Nature Energy, 5 (2020) 605-613.

[4] J. Lim, C.A. Fernández, S.W. Lee, M.C. Hatzell, Ammonia and Nitric Acid Demands for Fertilizer Use in 2050, ACS Energy Letters, 6 (2021) 3676-3685.

[5] K. Kim, A. Zagalskaya, J.L. Ng, J. Hong, V. Alexandrov, T.A. Pham, X. Su, Coupling nitrate capture with ammonia production through bifunctional redox-electrodes, Nat Commun, 14 (2023) 823.

[6] M.D.a.M.T.M. Koper, Powering denitrification-the perspectives of electrocatalytic nitrate reduction, Energy & Environmental Science, 5 (2012) 9726-9742.

[7] P.L. McCarty, What is the Best Biological Process for Nitrogen Removal: When and Why?, Environmental Science & Technology, 52 (2018) 3835-3841.

[8] L.F. Greenlee, Recycling fertilizer, Nature Energy, 5 (2020) 557-558.

[9] P.H. van Langevelde, I. Katsounaros, M.T.M. Koper, Electrocatalytic Nitrate Reduction for Sustainable Ammonia Production, Joule, 5 (2021) 290-294.

[10] A. Paliwal, C.D. Bandas, E.S. Thornburg, R.T. Haasch, A.A. Gewirth, Enhanced Nitrate Reduction Activity from Cu-Alloy Electrodes in an Alkaline Electrolyte, ACS Catalysis, 13 (2023) 6754-6762.

[11] D. Liu, L. Qiao, S. Peng, H. Bai, C. Liu, W.F. Ip, K.H. Lo, H. Liu, K.W. Ng, S. Wang, X. Yang, H. Pan, Recent Advances in Electrocatalysts for Efficient Nitrate Reduction to Ammonia, Advanced Functional Materials, (2023).

[12] S. Garcia-Segura, M. Lanzarini-Lopes, K. Hristovski, P. Westerhoff, Electrocatalytic reduction of nitrate: Fundamentals to full-scale water treatment applications, Applied Catalysis B: Environmental, 236 (2018) 546-568.

[13] Y. Wang, C. Wang, M. Li, Y. Yu, B. Zhang, Nitrate electroreduction: mechanism insight, in situ characterization, performance evaluation, and challenges, Chem Soc Rev, 50 (2021) 6720-6733.

[14] W. He, J. Zhang, S. Dieckhofer, S. Varhade, A.C. Brix, A. Lielpetere, S. Seisel, J.R.C. Junqueira, W. Schuhmann, Splicing the active phases of copper/cobalt-based catalysts achieves high-rate tandem electroreduction of nitrate to ammonia, Nat Commun, 13 (2022) 1129.

[15] S. Han, H. Li, T. Li, F. Chen, R. Yang, Y. Yu, B. Zhang, Ultralow overpotential nitrate reduction to ammonia via a three-step relay mechanism, Nature Catalysis, 6 (2023) 402-414.

[16] E. Murphy, Y. Liu, I. Matanovic, M. Rüscher, Y. Huang, A. Ly, S. Guo, W. Zang, X. Yan, A. Martini, J. Timoshenko, B.R. Cuenya, I.V. Zenyuk, X. Pan, E.D. Spoerke, P. Atanassov, Elucidating electrochemical nitrate and nitrite reduction over atomically-dispersed transition metal sites, Nature Communications, 14 (2023).

[17] F.Y. Chen, Z.Y. Wu, S. Gupta, D.J. Rivera, S.V. Lambeets, S. Pecaut, J.Y.T. Kim, P. Zhu, Y.Z. Finfrock, D.M. Meira, G. King, G. Gao, W. Xu, D.A. Cullen, H. Zhou, Y. Han, D.E. Perea, C.L. Muhich, H. Wang, Efficient conversion of low-concentration nitrate sources into ammonia on a Ru-dispersed Cu nanowire electrocatalyst, Nat Nanotechnol, 17 (2022) 759-767.

[18] Y. Wang, A. Xu, Z. Wang, L. Huang, J. Li, F. Li, J. Wicks, M. Luo, D.H. Nam, C.S. Tan, Y. Ding, J. Wu, Y. Lum, C.T. Dinh, D. Sinton, G. Zheng, E.H. Sargent, Enhanced Nitrate-to-Ammonia Activity on Copper-Nickel Alloys via Tuning of Intermediate Adsorption, J Am Chem Soc, 142 (2020) 5702-5708.

[19] J.-Y. Fang, Q.-Z. Zheng, Y.-Y. Lou, K.-M. Zhao, S.-N. Hu, G. Li, O. Akdim, X.-Y. Huang, S.-G. Sun, Ampere-level current density ammonia electrochemical synthesis using CuCo nanosheets simulating nitrite reductase bifunctional nature, Nature Communications, 13 (2022).

[20] Y. Bu, C. Wang, W. Zhang, X. Yang, J. Ding, G. Gao, Electrical Pulse‐Driven Periodic Self‐Repair of Cu‐Ni Tandem Catalyst for Efficient Ammonia Synthesis from Nitrate, Angewandte Chemie International Edition, 62 (2023).

[21] Q. Hu, Y. Qin, X. Wang, Z. Wang, X. Huang, H. Zheng, K. Gao, H. Yang, P. Zhang, M. Shao, C. He, Reaction intermediate-mediated electrocatalyst synthesis favors specified facet and defect exposure for efficient nitrate–ammonia conversion, Energy & Environmental Science, 14 (2021) 4989-4997.

[22] R. Daiyan, T. Tran-Phu, P. Kumar, K. Iputera, Z. Tong, J. Leverett, M.H.A. Khan, A. Asghar Esmailpour, A. Jalili, M. Lim, A. Tricoli, R.-S. Liu, X. Lu, E. Lovell, R. Amal, Nitrate reduction to ammonium: from CuO defect engineering to waste NOx-to-NH3 economic feasibility, Energy & Environmental Science, 14 (2021) 3588-3598.
[23] Z.-Y. Wu, M. Karamad, X. Yong, Q. Huang, D.A. Cullen, P. Zhu, C. Xia, Q. Xiao, M. Shakouri, F.-Y. Chen, J.Y. Kim, Y. Xia, K. Heck, Y. Hu, M.S. Wong, Q. Li, I. Gates, S. Siahrostami, H. Wang, Electrochemical ammonia synthesis via nitrate reduction on Fe single atom catalyst, Nature Communications, 12 (2021) 2870.
[24] Y. Xue, Q. Yu, Q. Ma, Y. Chen, C. Zhang, W. Teng, J. Fan, W.X. Zhang, Electrocatalytic Hydrogenation Boosts Reduction of Nitrate to Ammonia over Single-Atom Cu with Cu(I)-N(3)C(1) Sites, Environ Sci Technol, 56 (2022) 14797-14807.
[25] H. Yin, Y. Peng, J. Li, Electrocatalytic Reduction of Nitrate to Ammonia via a Au/Cu Single Atom Alloy Catalyst, Environ Sci Technol, 57 (2023) 3134-3144.
[26] S. Zhang, M. Li, J. Li, Q. Song, X. Liu, High-ammonia selective metal-organic framework-derived Co-doped Fe/Fe2O3 catalysts for electrochemical nitrate reduction, Proc Natl Acad Sci U S A, 119 (2022).
[27] K.-H. Kim, H. Lee, X. Huang, J.H. Choi, C. Chen, J.K. Kang, D. O'Hare, Energy-efficient electrochemical ammonia production from dilute nitrate solution, Energy & Environmental Science, 16 (2023) 663-672.
[28] X. Zou, J. Xie, C. Wang, G. Jiang, K. Tang, C. Chen, Electrochemical nitrate reduction to produce ammonia integrated into wastewater treatment: Investigations and challenges, Chinese Chemical Letters, 34 (2023) 107908.
[29] K. Flores, G.A. Cerrón-Calle, C. Valdes, A. Atrashkevich, A. Castillo, H. Morales, J.G. Parsons, S. Garcia-Segura, J.L. Gardea-Torresdey, Outlining Key Perspectives for the Advancement of Electrocatalytic Remediation of Nitrate from Polluted Waters, ACS ES&T Engineering, 2 (2022) 746-768.
[30] A. Atrashkevich, A.S. Fajardo, P. Westerhoff, W.S. Walker, C.M. Sanchez-Sanchez, S. Garcia-Segura, Overcoming barriers for nitrate electrochemical reduction: By-passing water hardness, Water Res, 225 (2022) 119118.
[31] W. Huang, M. Li, B. Zhang, C. Feng, X. Lei, B. Xu, Influence of operating conditions on electrochemical reduction of nitrate in groundwater, Water Environ Res, 85 (2013) 224-231.
[32] G. Jiang, M. Peng, L. Hu, J. Ouyang, X. Lv, Z. Yang, X. Liang, Y. Liu, H. Liu, Electron-deficient Cuδ+ stabilized by interfacial Cu–O-Al bonding for accelerating electrocatalytic nitrate conversion, Chemical Engineering Journal, 435 (2022) 134853.
[33] J. Sun, S. Garg, J. Xie, C. Zhang, T.D. Waite, Electrochemical Reduction of Nitrate with Simultaneous Ammonia Recovery Using a Flow Cathode Reactor, Environ Sci Technol, 56 (2022) 17298-17309.
[34] Z. Liu, F. Shen, L. Shi, Q. Tong, M.e. Tang, Y. Li, M. Peng, Z. Jiao, Y. Jiang, L. Ao, W. Fu, X. Lv, G. Jiang, L.a. Hou, Electronic Structure Optimization and Proton-Transfer Enhancement on Titanium Oxide-Supported Copper Nanoparticles for Enhanced Nitrogen Recycling from Nitrate-Contaminated Water, Environmental Science & Technology, 57 (2023) 10117-10126.
[35] W. Zheng, L. Zhu, Z. Yan, Z. Lin, Z. Lei, Y. Zhang, H. Xu, Z. Dang, C. Wei, C. Feng, Self-Activated Ni Cathode for Electrocatalytic Nitrate Reduction to Ammonia: From Fundamentals to Scale-Up for Treatment of Industrial Wastewater, Environ Sci Technol, 55 (2021) 13231-13243.
[36] W. Duan, Y. Chen, H. Ma, J.F. Lee, Y.J. Lin, C. Feng, In Situ Reconstruction of Metal Oxide Cathodes for Ammonium Generation from High-Strength Nitrate Wastewater: Elucidating the Role of the Substrate in the Performance of Co(3)O(4-x), Environ Sci Technol, 57 (2023) 3893-3904.
[37] A.I. Yanson, P. Rodriguez, N. Garcia-Araez, R.V. Mom, F.D. Tichelaar, M.T. Koper, Cathodic corrosion: a quick, clean, and versatile method for the synthesis of metallic nanoparticles, Angew Chem Int Ed Engl, 50 (2011) 6346-6350.
[38] Y. Chen, P. Ammari-Azar, H. Liu, J. Lee, Y. Xi, M.J. Castellano, S. Gu, W. Li, Sustainable waste-nitrogen upcycling enabled by low-concentration nitrate electrodialysis and high-performance ammonia electrosynthesis, EES Catalysis, 1 (2023) 504-515.
[39] X. Chen, T. Zhang, M. Kan, D. Song, J. Jia, Y. Zhao, X. Qian, Binderless and Oxygen Vacancies Rich FeNi/Graphitized Mesoporous Carbon/Ni Foam for Electrocatalytic Reduction of Nitrate, Environ Sci Technol, 54 (2020) 13344-13353.
[40] M.F. Islam, M.T. Islam, M.M. Hasan, M.M. Rahman, Y. Nagao, M.A. Hasnat, Facile fabrication of GCE/Nafion/Ni composite, a robust platform to detect hydrogen peroxide in basic medium via oxidation reaction, Talanta, 240 (2022) 123202.

[41] M.M. Waegele, C.M. Gunathunge, J. Li, X. Li, How cations affect the electric double layer and the rates and selectivity of electrocatalytic processes, The Journal of Chemical Physics, 151 (2019).
[42] M. Nurnobi Islam, M. Ahsan, K. Aoki, Y. Nagao, A.E. Alsafrani, H.M. Marwani, A. Almahri, M.M. Rahman, M.A. Hasnat, Development of CuNi immobilized Pt surface to minimize nitrite evolution during electrocatalytic nitrate reduction in neutral medium, Journal of Environmental Chemical Engineering, 11 (2023).
[43] B.C. Cornilsen, P.J. Karjala, P.L. Loyselle, Structural models for nickel electrode active mass, Journal of Power Sources, 22 (1988) 351-357.
[44] T.M. DeCarlo, Characterizing coral skeleton mineralogy with Raman spectroscopy, Nature Communications, 9 (2018) 5325.
[45] Y. Lei, B. Song, R.D. van der Weijden, M. Saakes, C.J.N. Buisman, Electrochemical Induced Calcium Phosphate Precipitation: Importance of Local pH, Environ Sci Technol, 51 (2017) 11156-11164.
[46] J. Sun, S. Garg, T.D. Waite, A Novel Integrated Flow-Electrode Capacitive Deionization and Flow Cathode System for Nitrate Removal and Ammonia Generation from Simulated Groundwater, Environmental Science & Technology, 57 (2023) 14726-14736.
[47] J.V. Perales-Rondon, D. Rojas, W. Gao, M. Pumera, Copper 3D-Printed Electrodes for Ammonia Electrosynthesis via Nitrate Reduction, ACS Sustainable Chemistry & Engineering, 11 (2023) 6923-6931.
[48] J.M. McEnaney, S.J. Blair, A.C. Nielander, J.A. Schwalbe, D.M. Koshy, M. Cargnello, T.F. Jaramillo, Electrolyte Engineering for Efficient Electrochemical Nitrate Reduction to Ammonia on a Titanium Electrode, ACS Sustainable Chemistry & Engineering, 8 (2020) 2672-2681.
[49] P. Li, L. Liao, Z. Fang, G. Su, Z. Jin, G. Yu, A multifunctional copper single-atom electrocatalyst aerogel for smart sensing and producing ammonia from nitrate, Proc Natl Acad Sci U S A, 120 (2023) e2305489120.
[50] J. Li, J. Gao, T. Feng, H. Zhang, D. Liu, C. Zhang, S. Huang, C. Wang, F. Du, C. Li, C. Guo, Effect of supporting matrixes on performance of copper catalysts in electrochemical nitrate reduction to ammonia, Journal of Power Sources, 511 (2021) 230463.
[51] F. Yao, M. Jia, Q. Yang, F. Chen, Y. Zhong, S. Chen, L. He, Z. Pi, K. Hou, D. Wang, X. Li, Highly selective electrochemical nitrate reduction using copper phosphide self-supported copper foam electrode: Performance, mechanism, and application, Water Res, 193 (2021) 116881.
[52] J. Zhou, F. Pan, Q. Yao, Y. Zhu, H. Ma, J. Niu, J. Xie, Achieving efficient and stable electrochemical nitrate removal by in-situ reconstruction of Cu2O/Cu electroactive nanocatalysts on Cu foam, Applied Catalysis B: Environmental, 317 (2022) 121811.
[53] M.J. Liu, J. Guo, A.S. Hoffman, J.H. Stenlid, M.T. Tang, E.R. Corson, K.H. Stone, F. Abild-Pedersen, S.R. Bare, W.A. Tarpeh, Catalytic Performance and Near-Surface X-ray Characterization of Titanium Hydride Electrodes for the Electrochemical Nitrate Reduction Reaction, J Am Chem Soc, 144 (2022) 5739-5744.
[54] I. Katsounaros, D. Ipsakis, C. Polatides, G. Kyriacou, Efficient electrochemical reduction of nitrate to nitrogen on tin cathode at very high cathodic potentials, Electrochimica Acta, 52 (2006) 1329-1338.
[55] J. Yao, Y. Mei, T. Yuan, J. Chen, H. Pan, J. Wang, Electrochemical removal of nitrate from wastewater with a Ti cathode and Pt anode for high efficiency and N2 selectivity, Journal of Electroanalytical Chemistry, 882 (2021).
[56] Y.-J. Shih, Z.-L. Wu, Electroplating of surfactant-modified tin catalyst over a nickel foam electrode (Sn/Ni) for selective N2 yield from nitrate reduction as affected by Sn(200) and Sn(101) crystal facets, Applied Catalysis B: Environmental, 285 (2021).
[57] H. Begum, M.N. Islam, S. Ben Aoun, J.A. Safwan, S.S. Shah, M.A. Aziz, M.A. Hasnat, Electrocatalytic reduction of nitrate ions in neutral medium at coinage metal-modified platinum electrodes, Environ Sci Pollut Res Int, 30 (2023) 34904-34914.
[58] Y. Bu, C. Wang, W. Zhang, X. Yang, J. Ding, G. Gao, Electrical Pulse-Driven Periodic Self-Repair of Cu-Ni Tandem Catalyst for Efficient Ammonia Synthesis from Nitrate, Angew Chem Int Ed Engl, 62 (2023) e202217337.
[59] C. Wang, F. Ye, J. Shen, K.-H. Xue, Y. Zhu, C. Li, In Situ Loading of Cu2O Active Sites on Island-like Copper for Efficient Electrochemical Reduction of Nitrate to Ammonia, ACS Applied Materials & Interfaces, 14 (2022) 6680-6688.
[60] S.A. Akhade, I.T. McCrum, M.J. Janik, The Impact of Specifically Adsorbed Ions on the Copper-Catalyzed Electroreduction of CO2, Journal of The Electrochemical Society, 163 (2016) F477.

[61] I. Katsounaros, G. Kyriacou, Influence of the concentration and the nature of the supporting electrolyte on the electrochemical reduction of nitrate on tin cathode, Electrochimica Acta, 52 (2007) 6412-6420.
[62] B.H.R. Suryanto, H.-L. Du, D. Wang, J. Chen, A.N. Simonov, D.R. MacFarlane, Challenges and prospects in the catalysis of electroreduction of nitrogen to ammonia, Nature Catalysis, 2 (2019) 290-296.

Figure Captions

Fig. 1 Electrochemical nitrate reduction with Ni foam cathode. **a**, Influence of Ca^{2+} and bicarbonate on nitrate removal over ten-cycle recycling. **b**–**c**, XRD patterns (**b**) and Raman spectrum (**c**) of fresh and used Ni foam under different ion compositions. **d**, Evolution of NH_4^+, NO_2^-, NO_3^-, and other nitrogen species in nitrate-only conditions. **e**–**f**, LSV curves (**e**) and Nyquist plots (**f**) of fresh and used Ni foam under different test conditions, both LSV and EIS were recorded with electrolytes containing 50 mM Na_2SO_4 and 4 mM $NaNO_3$. **g**–**h**, SEM images of fresh (**g**) and used (**h**) Ni foam in NO_3^- condition. **i**–**j**, O 1s and Ni 2p XPS spectra of fresh (**i**) and used (**j**) Ni foam in nitrate-only condition. **CPE**, constant phase element, $\mathbf{R_{ct}}$, charge transfer resistance, $\mathbf{R_s}$, resistance of bulk solution.

Fig. 2 Influence of ion composition. a–**c**,The evolution of NH_4^+, NO_2^-, NO_3^-, and other nitrogen species in NO_3^- + Ca^{2+} (**a**), NO_3^- + HCO_3^- (**b**), and NO_3^- + Ca^{2+} + HCO_3^- (**c**) condition. **d**–**f**, SEM images of used Ni foam in NO_3^- + Ca^{2+} (**d**), NO_3^- + HCO_3^- (**e**), and NO_3^- + Ca^{2+} + HCO_3^- (**f**) condition. **g**, O 1s and Ni 2p XPS spectra of Ni foam in NO_3^- + Ca^{2+}, NO_3^- + HCO_3^-, and NO_3^- + Ca^{2+} + HCO_3^- condition.

Fig. 3 Influence of cathode material. a, Electrochemical nitrate removal with Cu foam, Ti plate, and Sn plate electrodes in nitrate-only solution over a ten-cycle test. **b**, LSV curves of Cu foam, Ti plate, and Sn plate in the absence or presence of 4 mM NO_3^-; 50 mM Na_2SO_4 were added as supporting electrolytes. **c**–**e**, The determination of double layer capacitance of Cu foam (**c**), Ti plate (**d**), and Sn plate (**e**) under fresh and NO_3^- conditions. **f**–**h**, XRD patterns of Cu foam (**f**), Ti plate (**g**), and Sn plate (**h**) in nitrate-only condition.

Fig. 4 Joint effects of coexisting ions and cathode material. a–**c**, Electrochemical nitrate reduction with Cu foam (**a**), Ti plate (**b**), and Sn plate (**c**) in the presence of different ions over a ten-cycle test. **d**–**f**, LSV curves of Cu foam (**d**), Ti plate (**e**), and Sn plate (**f**) under different ion compositions. **g**–**i**, The Nyquist plots for the EIS spectra of Cu foam (**g**), Ti plate (**h**), and Sn plate (**i**) under different ion compositions. LSV and EIS were collected with electrolytes containing 50 mM Na_2SO_4 and 4 mM $NaNO_3$. **CPE**, constant phase element, $\mathbf{R_{ct}}$, charge transfer resistance, $\mathbf{R_s}$, resistance of bulk solution.

Fig. 5 Long-term performance. **a**, Nitrate removal efficiency over continuous flow operation mode in treating simulated water, nitrate spiked tap water, and actual nitrate-polluted groundwater. **b**–**c**, XRD patterns of used Cu foam in simulated water (**b**) and groundwater (**c**). **d**, Change of Ca^{2+} and Mg^{2+} concentration over tests with nitrate-polluted groundwater. The same Cu foam cathode was used for the tests with synthetic nitrate-containing water. For the tests with nitrate-spiked tap water and actual nitrate-polluted groundwater, new Cu foams were

800 introduced.

801

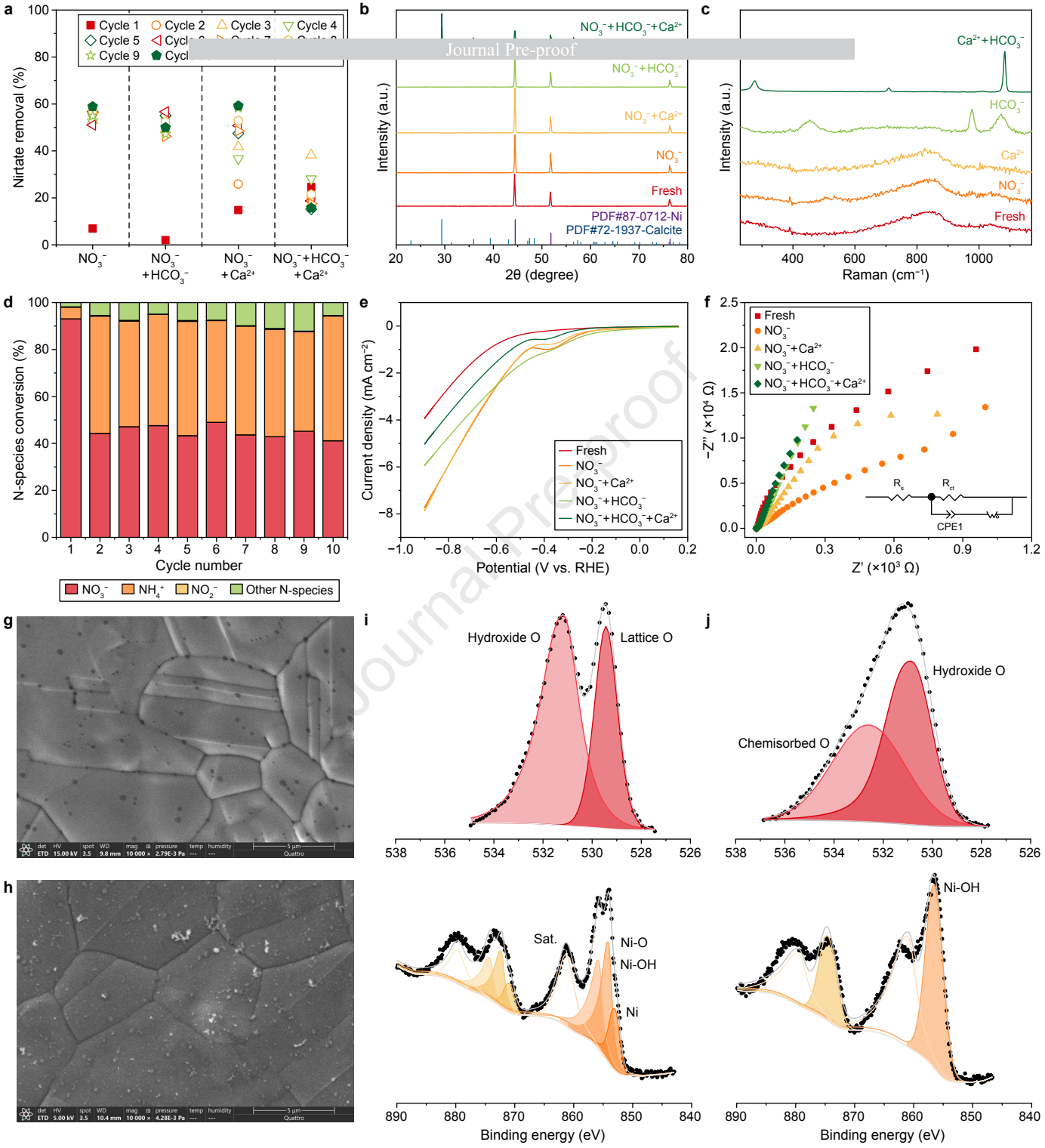

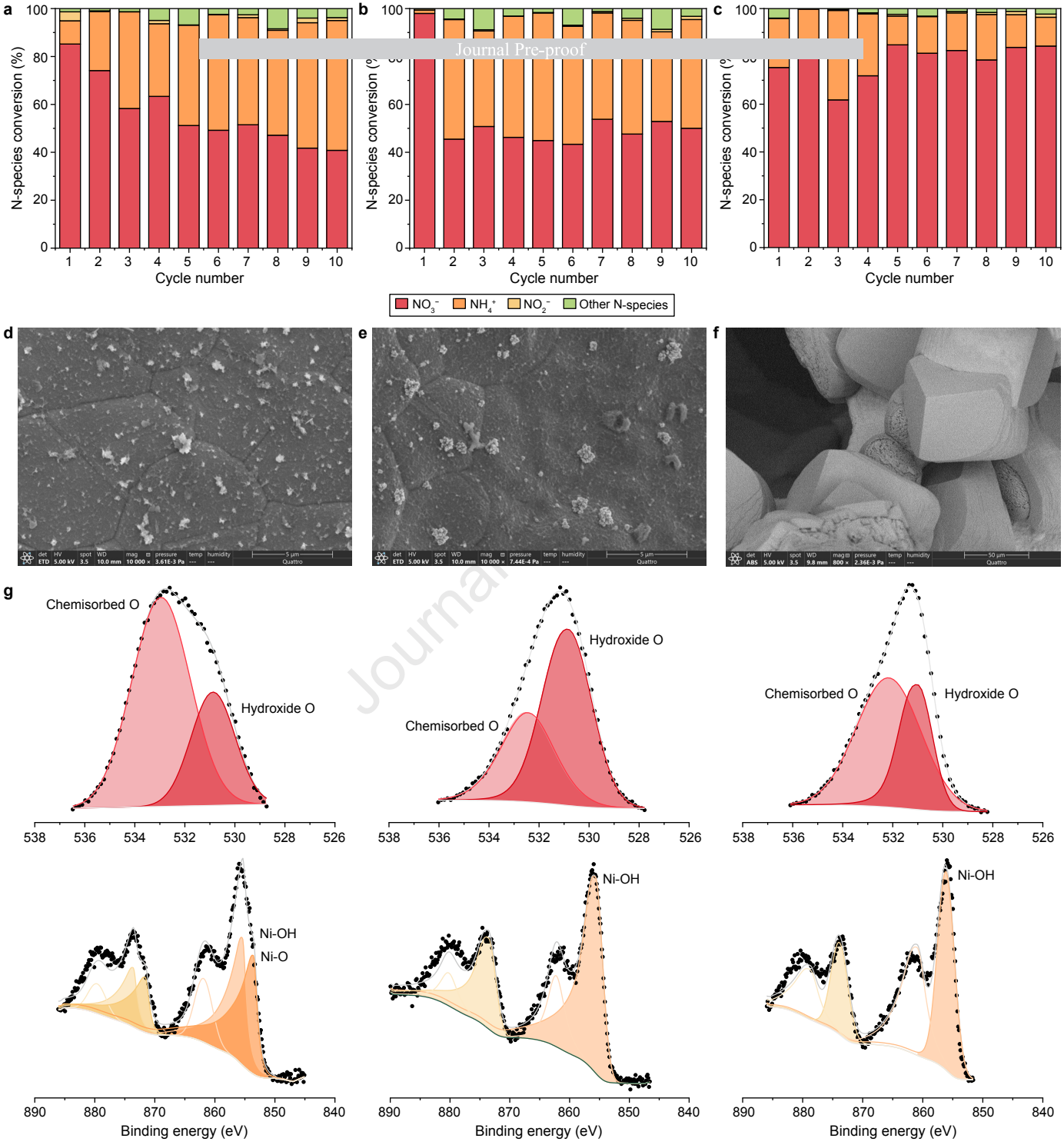

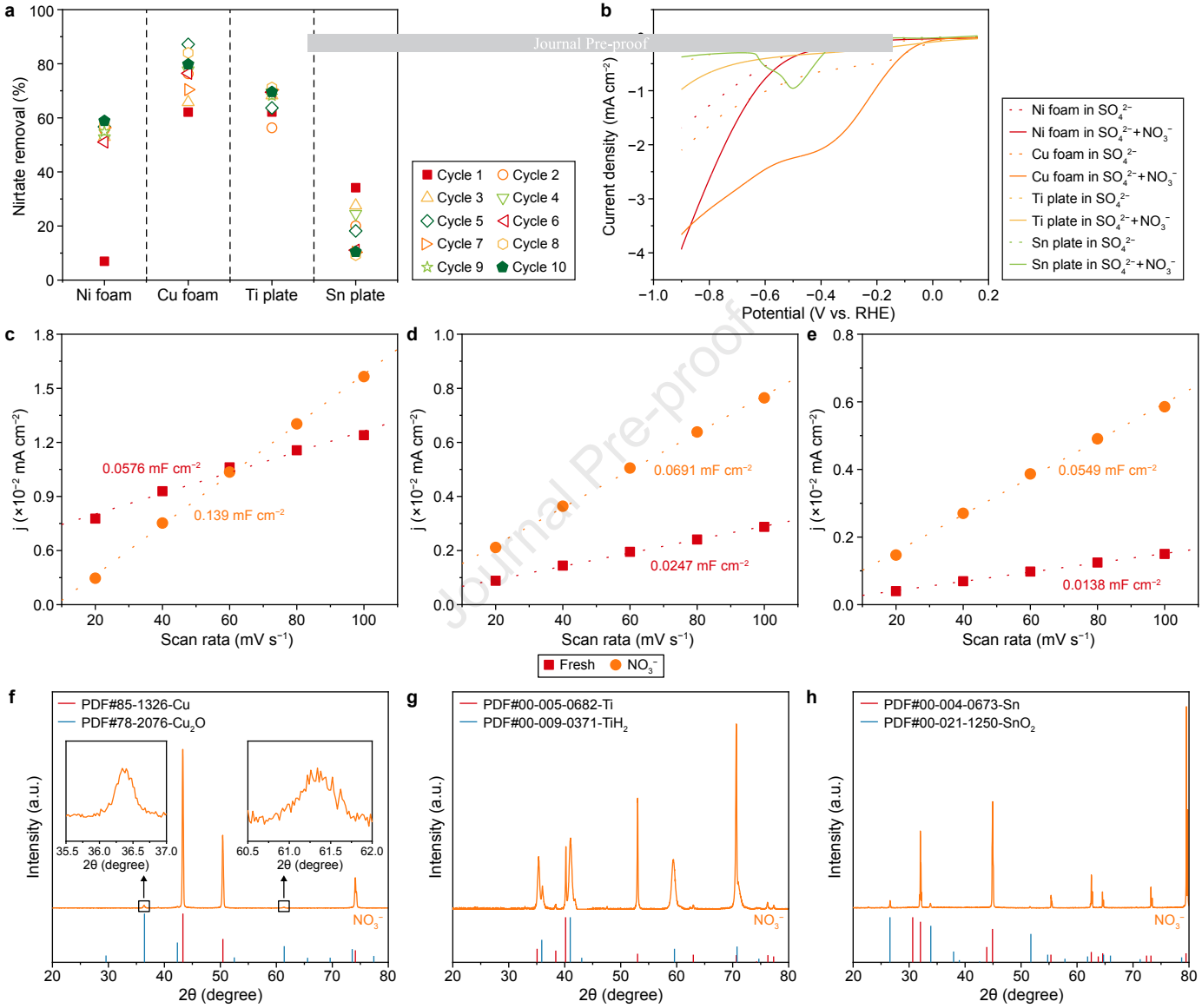

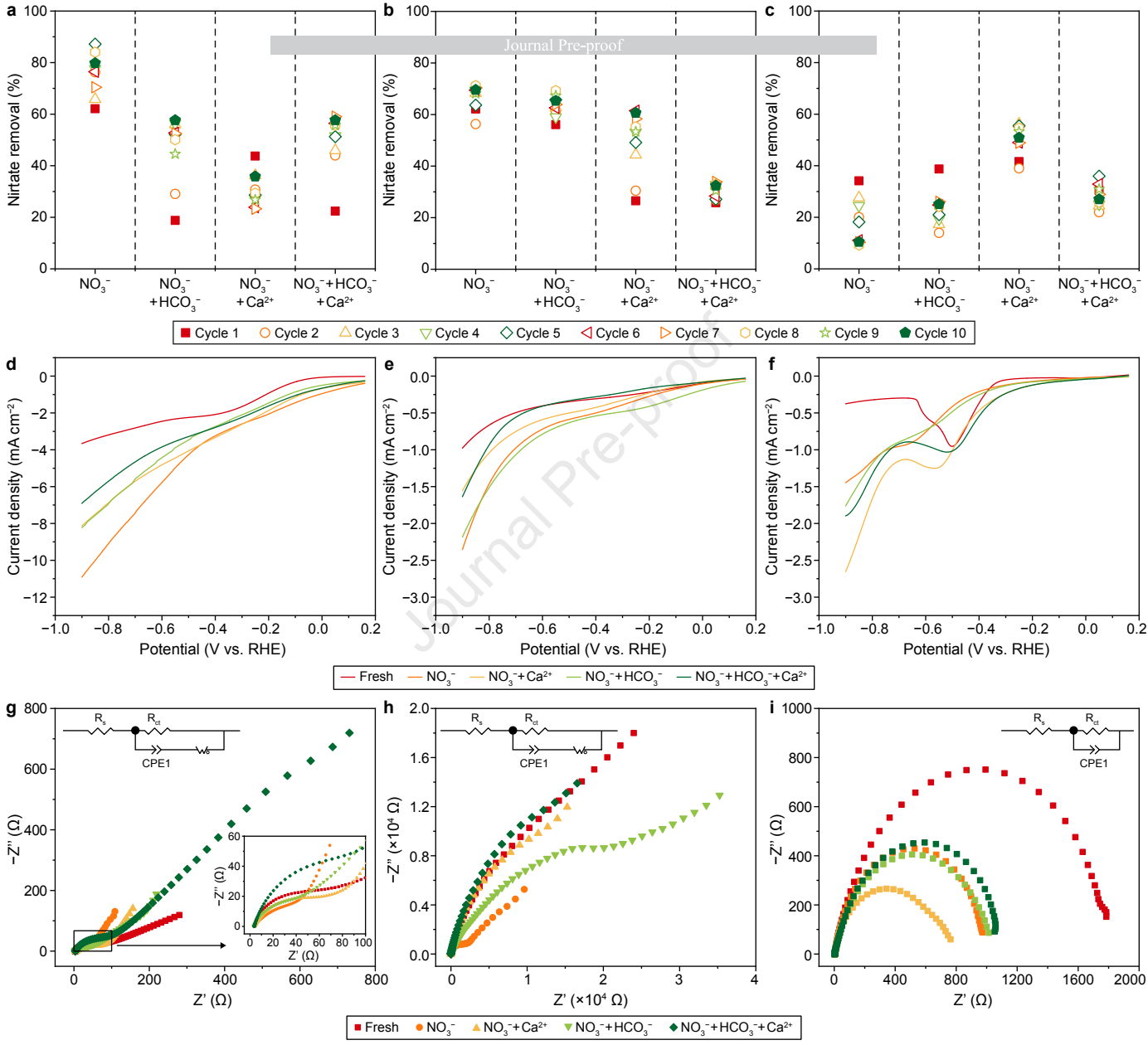

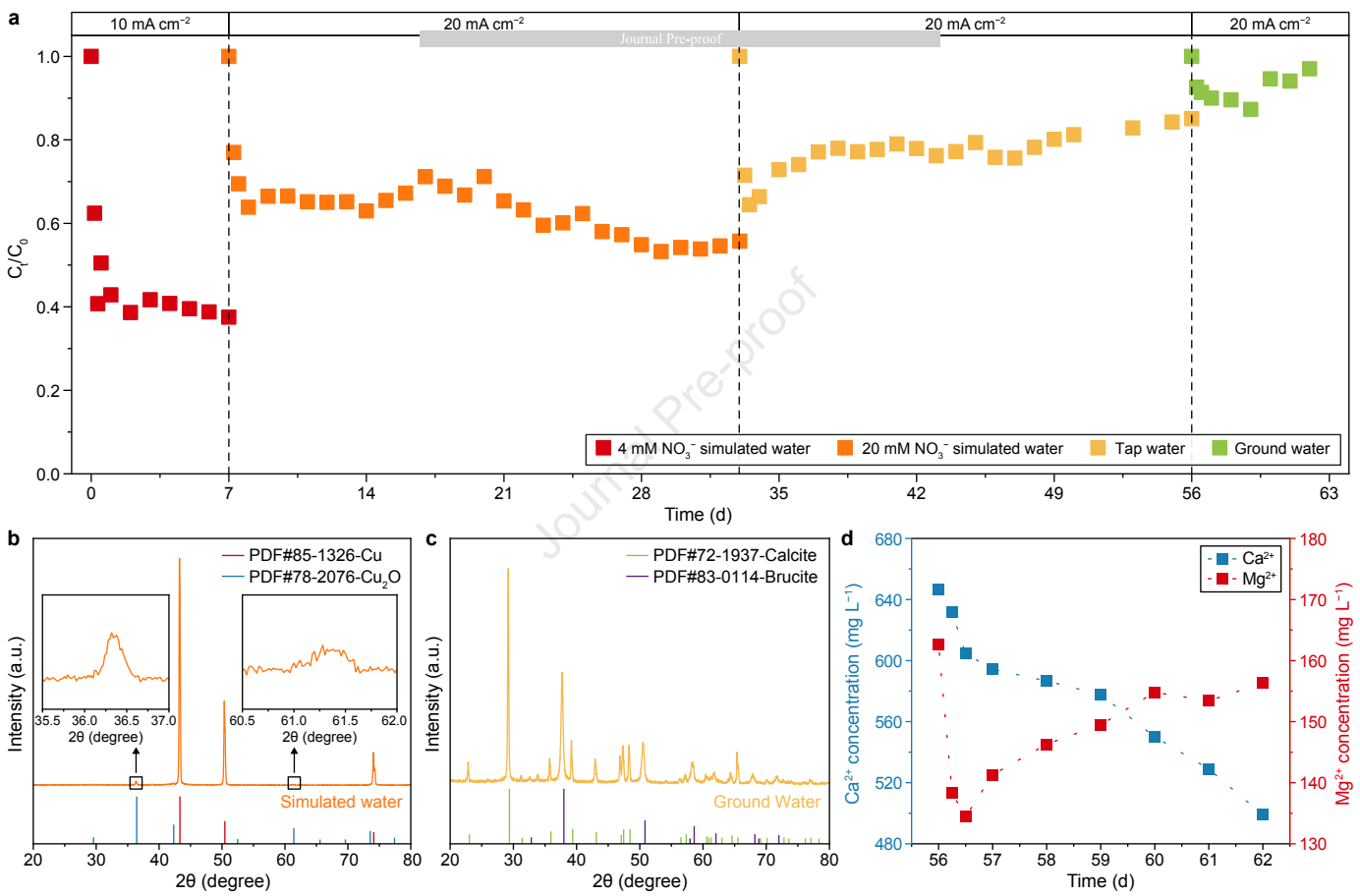
a
10 mA cm⁻²
20 mA cm⁻²
20 mA cm⁻²
20 mA cm⁻²
Journal Pre-proof
C_t/C_0
Time (d)
4 mM NO3⁻ simulated water
20 mM NO3⁻ simulated water
Tap water
Ground water
b
PDF#85-1326-Cu
PDF#78-2076-Cu2O
Intensity (a.u.)
2θ (degree)
Simulated water
c
PDF#72-1937-Calcite
PDF#83-0114-Brucite
Ground Water
d
Ca2+
Mg2+
Ca2+ concentration (mg L⁻¹)
Mg2+ concentration (mg L⁻¹)
Time (d)

Highlights

- In-situ evolution of Cu, Ni, Ti and Sn cathodes occurs via cathodic corrosion.
- In-situ activation of Ni or Cu cathode enhances electrocatalytic-nitrate reduction.
- Ca^{2+} promotes nitrate removal by complexation and condensing electric double layer.
- Cathode scaling inhibits electrochemical nitrate removal over long-term operation.

Declaration of interests

☒ The authors declare that they have no known competing financial interests or personal relationships that could have appeared to influence the work reported in this paper.

☐ The authors declare the following financial interests/personal relationships which may be considered as potential competing interests: